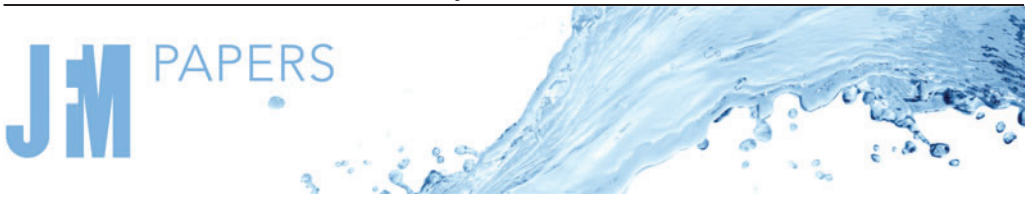
J. Fluid Mech. (2022), *vol*. 941, A50, doi:10.1017/jfm.2022.309



A drop in a nonlinear shear flow

Moshe Favelukis†

Department of Chemical Engineering, Shenkar – College of Engineering and Design, Ramat-Gan, 5252626, Israel

(Received 18 August 2021; revised 30 December 2021; accepted 1 April 2022)

The fluid mechanics problem of an initially spherical drop subjected to a two-directional nonlinear cubic shear flow, under creeping flow conditions, is theoretically studied. This physical situation is described by four dimensionless numbers: the capillary number (Ca), the viscosity ratio (λ), the linear velocity ratio (G) and the nonlinear intensity of the flow (E). Analytical expressions for the external and internal flows of a spherical drop as well as for the shape of the deformed drop were obtained by applying Lamb's general solution to the Stokes equations. The internal and external streamlines of a spherical drop ($Ca = 0$) suggest interesting and unusual shapes which are sometimes also accompanied by many stagnation points. When $\lambda = \infty$, the drop becomes a solid sphere with an angular velocity $\omega = -(1 - G)/2$ independent of E. For the familiar simple shear flow in the x-direction ($G = 0, E = 0$), Taylor's theory, valid at $Ca \ll 1$ and $\lambda = O(1)$, predicts an ellipsoidal drop oriented at an azimuthal angle $\phi = 45°$; as Ca increases, the deformation increases and the drop attains a peanut shape. For other linear or nonlinear cases, the drop is aligned at $\phi = \pm 45°$, and a spherical drop with no deformation is possible at $Ca \neq 0$. In a highly viscous drop ($\lambda \gg 1$), the drop remains almost spherical even at $Ca = O(1)$, oriented at $\phi = 0°$ or $90°$ ($G \neq 1$), and its deformation is independent of Ca.

Key words: drops and bubbles, low-Reynolds-number flows

1. Introduction

A large number of industrial products take the form of emulsions in which a drop of one fluid is suspended in a liquid of another fluid. Often, these emulsions are processed in rotary equipment generating shear or extensional flows, resulting in the deformation or the breakup of the embedded drops. Thus, the fluid mechanics problem of a drop undergoing shear or extensional flow has a long history and important place in science since the pioneering work of Taylor (1932, 1934). Since then, and for the last ninety years, this subject has been considered by numerous researchers who refined the theory and the experimental results. Many of these studies, as well as industrial applications, can be found

† Email address for correspondence: favelukis@gmail.com

© The Author(s), 2022. Published by Cambridge University Press

https://doi.org/10.1017/jfm.2022.309 Published online by Cambridge University Press

the reviews of Acrivos (1983, 1990), Rallison (1984), Stone (1994) and Briscoe, Lawrence & Mietus (1999), and in the books of Clift, Grace & Weber (1978), Sadhal, Ayyaswamy & Chung (1997), Zapryanov & Tabakova (1999), Polyanin *et al.* (2002) and Leal (2007).

Consider a non-buoyant spherical drop (radius a, viscosity μ_{in}) suspended in another fluid (viscosity μ) which is subjected to a simple (linear) shear flow. Let the two fluids be Newtonian, incompressible, immiscible and under creeping flow conditions. This situation, described by the Stokes equations, is governed by two dimensionless parameters. These are: the capillary number, $Ca = \mu A a/\sigma$, the ratio of the external viscous force, which tends to deform the drop, to the surface tension force, which tends to keep the drop spherical; and the viscosity ratio, $\lambda = \mu_{in}/\mu$. Here, A is the shear rate of the undisturbed motion and σ is the surface tension. The present theoretical report deals with small deformations ($Ca \ll 1$ and $\lambda = O(1)$, or $Ca = O(1)$ and $\lambda \gg 1$), where the drop can be considered a slightly perturbed sphere. There is, however, another regime of large deformations ($Ca \gg 1$ and $\lambda \ll 1$), where slender drops with pointed ends are observed, which will not be covered in this communication.

Like many other topics in fluid mechanics, the first one to explore, both theoretically and experimentally, the deformation of a drop in a simple (linear) shear and creeping flow was Taylor (1932, 1934). By applying Lamb's general solution to the Stokes equations, Taylor (1932) obtained the $O(Ca^0)$ (spherical) solution, and extended the Einstein (1906, 1911) suspension viscosity relation to the case of a dilute emulsion. According to Taylor (1934), when $Ca \ll 1$ and $\lambda = O(1)$, the $O(Ca^1)$ deformed shape is an ellipsoid oriented along the principal axis of elongation at an angle of 45° with the direction of the flow. Taylor also observed that, in a simple shear flow, small drop deformations can also be achieved at $Ca = O(1)$, as long as the drop is very viscous ($\lambda \gg 1$). Taylor (1934) modified his theory to find out that in this case the drop is positioned with the direction of the flow, its shape depends on λ but not on Ca, and breakup is not possible.

Bartok & Mason (1958) obtained expressions for external and internal streamlines in the $z = 0$ plane, explored their shapes and calculated their mean time of circulation. Chaffey, Brenner & Mason (1965*a*), confirmed Taylor's results, and also explored the behaviour of a drop in a non-uniform linear shear flow between counter-rotating disks. Taylor's theory was refined by Cox (1969), who also include studies on the behaviour of the drop when the shear flow started impulsively from rest. Rallison (1980, 1981) suggested a comprehensive procedure for any kind of linear flow, and performed a numerical investigation for the specific case where the drop and the continuous phase have the same viscosity ($\lambda = 1$). Hetsroni & Haber (1970) assumed the undisturbed motion to be arbitrary and duplicated Taylor's results for the case of a simple shear flow. Wall bounded (Chaffey, Brenner & Mason 1965*b*, 1967), and unbounded (Chaffey & Brenner 1967) Couette flow studies, lead to the $O(Ca^1)$ velocity profile and to the $O(Ca^2)$ deformed shape. Accordingly, the drop deviates from its ellipsoidal shape and the angle between the maximum drop elongation and the direction of the flow is smaller than 45° and approaches 0° at larger Ca and λ. A general linear flow field method for the $O(Ca^2)$ deformed shape was also suggested by Barthès-Biesel & Acrivos (1973). Their analysis predicts that low viscosity ($\lambda < 0.1$) or high viscosity drops ($\lambda > 3.6$) behave like the $O(Ca^1)$ deformed theory, and their shapes are stable to small disturbances. For medium viscosity drops ($0.1 < \lambda < 3.6$) there is a critical value of Ca (the breakup point) beyond which no solution exists. Vlahovska, Blawzdziewicz & Loewenberg (2009) developed a small deformation perturbation analysis, extended the Barthès-Biesel & Acrivos (1973) solution and obtained the $O(Ca^3)$ deformed shape.

https://doi.org/10.1017/jfm.2022.309 Published online by Cambridge University Press

Experiments which verify the main predictions of the small deformation theory were conducted by Taylor (1934), Bartok & Mason (1959), Rumscheidt & Mason (1961*a*,*b*), Karam & Bellinger (1968), Torza, Cox & Mason (1972), Grace (1982), Guido, Greco & Villone (1999), Guido, Simeone & Alfani (2002), Guido & Greco (2001), Rust & Manga (2002), Megías-Alguacil, Fischer & Windhab (2004, 2006), Megías-Alguacil *et al.* (2005), Vananroye, van Puyvelde & Moldenaers (2011) and others. Excellent agreement between the experiments and the $O(Ca^1)$ deformation theory was obtained at very low capillary numbers. At slightly higher capillary numbers, the predictions of the $O(Ca^2)$ deformation theory (change in orientation and drop shape) were also qualitatively confirmed. Many of these publications also contain breakup mechanisms studies, which appear to depend not only on Ca and λ, but also on the initial drop shape and on the rate of increase of the shear rate up to the critical value. Usually, breakup is by centre pinching, leaving two large drops separated by tinny satellite droplets. Another breakup mechanism is called tip streaming, where very small drops are detached from the drop at the tip of the drop. The literature suggests that tip streaming, usually observed in highly elongated drops, is caused by surfactants moving in the direction of the tip of the drop and accumulating there (De Bruijn 1993).

Over the years, Taylor's theory was not only reconfirmed by theory and experiments in a large number of reports, but also many extensions have been suggested to it. Bentley & Leal (1986) used a computer controlled four-roll mill apparatus to study the effect of vorticity. They considered linear flows between simple shear flow, where the magnitude of the vorticity is equal to that of the shear rate, and two-dimensional hyperbolic flow, where vorticity is absent. In general, the effect of vorticity is to inhibit the deformation and the breakup of drops (Rallison 1981). Hakimi & Schowalter (1980) explored the flow produced in an orthogonal rheometer (eccentric parallel rotating discs). Similar to simple shear flow, the flow contains angular deformation and vorticity. Contrary to simple shear flow, deformation and vorticity can be controlled independently. Other extensions to Taylor's theory, which are not directly connected to the present analytical report include: the effects of wall confinement, effects of inertia, non-Newtonian systems, transient response to a start-up shear flow, drop relaxation after the shear flow has been stopped, oscillatory shear flows, addition of surfactants, capsules made of liquid drops enclosed by elastic membranes, heat or mass transfer, electrical or magnetic fields as well as different numerical methods.

So far, we dealt with the behaviour of a slightly deformed drop subjected to a simple (linear) shear flow under creeping flow conditions. However, rotating equipment which processes emulsions does not necessarily produce linear flows, such as uniaxial or biaxial extensional flows, hyperbolic flow or simple shear flow, which were extensively treated in the literature. Instead, it is expected to find in this type of machinery more complicated flows which include nonlinear terms to the velocity field. For example, Antanovskii (1996) considered a pointed drop in a two-dimensional nonlinear extensional flow, since it describes better (than the linear flow) the flow produced in Taylor's four-roller mill apparatus. Nonlinear flows are also expected in microfluidic devices, where the size of the drop is comparable to that of the apparatus (Pozrikidis 1998; Dimitrakopoulos 2017). Sherwood (1984) and Favelukis (2016, 2019*a*,*b*) suggested a nonlinear uniaxial extensional flow in their slender drop studies. Sherwood's (1984) velocity profile, which combines linear and cubic terms, but not quadratic terms in order to maintain the symmetry of the drop, has been recently adopted by Favelukis (2017, 2019*c*, 2020) in order to explore small drop deformations in a nonlinear extensional creeping flow. As expected, the inclusion of nonlinear terms results in more deformation and breakup patterns than the linear case.

https://doi.org/10.1017/jfm.2022.309 Published online by Cambridge University Press

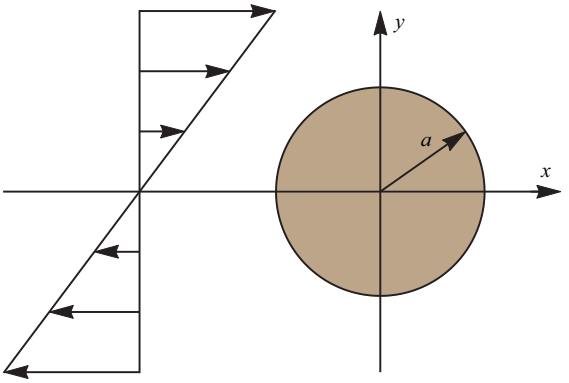


Figure 1. A spherical drop in a simple (linear) shear flow ($A > 0$, $B = C = 0$).

The nonlinear examples listed here are limited to extensional flows, whereas the objective of this report is to explore the behaviour of a drop in a nonlinear shear flow. Apart from simple shear flow, Hetsroni & Haber (1970), Chan & Leal (1979) and Yang & Lee (1989) also explored small drop deformations in Poiseuille flow which can be considered as a nonlinear shear flow. However, since Poiseuille flow consists of quadratic velocity terms, the deformation of the drop lacks symmetry around the origin. It is therefore the purpose of this theoretical report to extend the nonlinear literature, by exploring small deformations of a drop in a two-directional nonlinear cubic shear flow under creeping flow conditions.

2. The governing equations

Figure 1 describes an initially non-buoyant spherical drop (radius a) of one fluid positioned at the origin of a coordinate system and submerged in another fluid. Let both fluids be immiscible, incompressible, Newtonian and under creeping flow conditions. Far away from the drop, the external fluid experiences a nonlinear cubic shear flow (in two directions), defined in Cartesian coordinates (x, y, z) as

$$v_x = Ay + By^3, \tag{2.1}$$

$$v_y = Cx + Bx^3, \tag{2.2}$$

$$v_z = 0, \tag{2.3}$$

$$p = 6\mu Bxy + K. \tag{2.4}$$

Here, p is the pressure, μ is the viscosity of the external fluid and K is an arbitrary constant. Note that quadratic terms are missing in order to maintain an odd velocity profile around the origin. The constants A, B and C can attain positive, negative or zero values, and if $B = C = 0$, and $A > 0$, the familiar simple (linear) shear flow, described in figure 1, is recovered. Furthermore, the constants of the terms with the cubic powers must be the same, otherwise the Stokes equations cannot be fulfilled. Similar to simple shear flow, this nonlinear shear flow possesses angular deformation and rotation but not linear deformation.

https://doi.org/10.1017/jfm.2022.309 Published online by Cambridge University Press

In spherical coordinates (r, θ, ϕ), with $0 \leq \theta \leq \pi$ being the polar angle and $0 \leq \phi < 2\pi$ the azimuth angle, the undisturbed motion, given by (2.1)–(2.4), reads

$$v_r = \tfrac{1}{2}(A + C)r\sin^2\theta \sin(2\phi) + \tfrac{1}{2}Br^3\sin^4\theta \sin(2\phi), \tag{2.5}$$

$$v_\theta = \tfrac{1}{2}(A + C)r\cos\theta \sin\theta \sin(2\phi) + \tfrac{1}{2}Br^3 \cos\theta\sin^3\theta \sin(2\phi), \tag{2.6}$$

$$v_\phi = \tfrac{1}{2}r\sin\theta[-A + C + (A + C)\cos(2\phi)] + Br^3\sin^3\theta \cos(2\phi), \tag{2.7}$$

$$p = 3\mu Br^2\sin^2\theta \sin(2\phi) + K. \tag{2.8}$$

The Stokes equations, outside and inside the drop, together with the appropriate boundary conditions, suggest a problem which is governed by four dimensionless parameters. These are: the capillary number (Ca), the viscosity ratio (λ), the linear velocity ratio (G) and the nonlinear intensity of the flow (E)

$$Ca = \frac{\mu A a}{\sigma}, \tag{2.9}$$

$$\lambda = \frac{\mu_{in}}{\mu}, \tag{2.10}$$

$$G = \frac{C}{A}, \tag{2.11}$$

$$E = \frac{Ba^2}{A}. \tag{2.12}$$

Here, μ and μ_{in} are the external and internal viscosities, respectively, a is the initial radius of the spherical drop and σ is the surface tension. Note that since the constants A, B and C can be positive, negative or zero, this suggests the same for Ca, G and E.

From now on and in what follows, we non-dimensionalize the lengths with the initial drop radius (a), the velocities with the characteristic linear velocity ($U = Aa$) and the pressures and viscous stresses with the characteristic external stress (μA). A general solution the Stokes equations, in spherical coordinates, was suggested by Lamb (1945), see also Happel & Brenner (1983) and Zapryanov & Tabakova (1999). For the internal flow have

$$\boldsymbol{v}_{in} = \sum_{n=1}^{\infty}\left[\frac{(n+3)r^2\nabla p_{n,in}}{2\lambda(n+1)(2n+3)} - \frac{nr\boldsymbol{e}_r p_{n,in}}{\lambda(n+1)(2n+3)} + \nabla\Phi_{n,in} + \nabla\times(r\boldsymbol{e}_r\chi_{n,in})\right], \tag{2.13}$$

$$p_{in} = p_0 + \sum_{n=1}^{\infty} p_{n,in}, \tag{2.14}$$

$$p_{n,in} = r^n\sum_{m=0}^{n} P_n^m(\eta)[a_{n,m}\cos(m\phi) + b_{n,m}\sin(m\phi)], \tag{2.15}$$

$$\Phi_{n,in} = r^n\sum_{m=0}^{n} P_n^m(\eta)[c_{n,m}\cos(m\phi) + d_{n,m}\sin(m\phi)], \tag{2.16}$$

$$\chi_{n,in} = r^n\sum_{m=0}^{n} P_n^m(\eta)[e_{n,m}\cos(m\phi) + f_{n,m}\sin(m\phi)]. \tag{2.17}$$

https://doi.org/10.1017/jfm.2022.309 Published online by Cambridge University Press

And by replacing n with $-(n+1)$, we arrive at the external flow expressions

$$\boldsymbol{v}_{out} = \boldsymbol{v}_\infty + \sum_{n=1}^{\infty}\left[-\frac{(n-2)r^2\nabla p_{n,out}}{2n(2n-1)} + \frac{(n+1)r\boldsymbol{e}_r p_{n,out}}{n(2n-1)} + \nabla\Phi_{n,out} + \nabla\times(r\boldsymbol{e}_r\chi_{n,out})\right], \tag{2.18}$$

$$p_{out} = p_\infty + \sum_{n=1}^{\infty} p_{n,out}, \tag{2.19}$$

$$p_{n,out} = r^{-n-1}\sum_{m=0}^{n} P_n^m(\eta)[a_{-n-1,m}\cos(m\phi) + b_{-n-1,m}\sin(m\phi)], \tag{2.20}$$

$$\Phi_{n,out} = r^{-n-1}\sum_{m=0}^{n} P_n^m(\eta)[c_{-n-1,m}\cos(m\phi) + d_{-n-1,m}\sin(m\phi)], \tag{2.21}$$

$$\chi_{n,out} = r^{-n-1}\sum_{m=0}^{n} P_n^m(\eta)[e_{-n-1,m}\cos(m\phi) + f_{-n-1,m}\sin(m\phi)]. \tag{2.22}$$

Here, $\boldsymbol{v}$ is the velocity, $\boldsymbol{v}_\infty$ and p_∞ are the velocity vector and pressure of the unperturbed motion, p_0 is the internal pressure in the absence of flow, $\boldsymbol{e}_r$ is the unit vector in the radial direction and the subscripts in and out represent inside and outside the drop, respectively. The functions p_n, Φ_n and χ_n are solid spherical harmonics with $P_n^m(\eta)$ being the associated Legendre polynomials of degree n and order m, and the usual substitution in spherical coordinates ($\eta = \cos\theta$) has been made. The constants in (2.15)–(2.17) and (2.20)–(2.22) are to be evaluated according to the usual boundary conditions suggested by the literature.

The no slip condition requires equal velocities at the interface ($r = 1$). Furthermore, in a stationary drop the normal velocities also vanish:

$$v_{r,out} = v_{r,in} = 0, \tag{2.23}$$

$$v_{\theta,out} = v_{\theta,in}, \tag{2.24}$$

$$v_{\phi,out} = v_{\phi,in}. \tag{2.25}$$

Newton's third law of motion requires the normal and tangential stresses of the two fluids to be balanced at the interface ($r = 1$). For the tangential stress we have

$$\tau_{r\theta,out} = \tau_{r\theta,in}, \tag{2.26}$$

$$\tau_{r\phi,out} = \tau_{r\phi,in}. \tag{2.27}$$

According to the method for solving this type of problem, (2.13)–(2.27) are sufficient to obtain the spherical solution $O(Ca^0)$. This zeroth-order solution can then be substituted into the normal stress balance at the interface to obtain the first-order, $O(Ca^1)$, deformed shape

$$p_{in} - p_{out} + \tau_{rr,out} - \tau_{rr,in} = \frac{1}{Ca}\left(\frac{1}{R_1} + \frac{1}{R_2}\right), \tag{2.28}$$

where R_1 and R_2 are the principal radii of curvature of the surface.

https://doi.org/10.1017/jfm.2022.309 Published online by Cambridge University Press

3. The undisturbed motion

In order to better understand this physical situation, it is worthwhile to describe first the behaviour of the undisturbed motion, that is, the flow in the absence of the drop. Since the undisturbed motion is an incompressible two-dimensional flow, we can easily define and obtain for it a dimensionless streamfunction

$$v_x = +\frac{\partial \psi}{\partial y} = y + Ey^3, \tag{3.1}$$

$$v_y = -\frac{\partial \psi}{\partial x} = Gx + Ex^3, \tag{3.2}$$

$$\psi = \frac{1}{2}(y^2 - Gx^2) + \frac{E}{4}(y^4 - x^4). \tag{3.3}$$

Note that v_x vanishes at $y = 0$ or $y = \pm i/\sqrt{E}$, while v_y vanishes at $x = 0$ or $x = \pm i\sqrt{G/E}$.

In terms of the strain rate tensor ($\boldsymbol{\Gamma}$) and the vorticity tensor ($\boldsymbol{\Omega}$), the only non-vanishing components are

$$\Gamma_{xy} = \Gamma_{yx} = \tfrac{1}{2}[(1 + G) + 3E(x^2 + y^2)], \tag{3.4}$$

$$\Omega_{xy} = -\Omega_{yx} = \tfrac{1}{2}[(G - 1) + 3E(x^2 - y^2)]. \tag{3.5}$$

Thus, for a linear shear flow ($E = 0$), if $G = 0$ we have the familiar simple shear flow in the x-direction with both angular deformation and rotation of the same magnitude, if $G = 1$ there is only angular deformation and if $G = -1$ there is only rotation. In a nonlinear shear flow ($E \neq 0$), there will be always angular deformation and rotation simultaneously.

Figure 2 shows the velocity vector of the unperturbed motion for the case where the shear flow is linear ($E = 0$). Four G cases are described: the familiar simple shear flow in which the velocity is in the x-direction ($G = 0$) or in the y-direction ($G = \infty$); a positive case ($G = 1$), where observing at an angle of $\phi = 45°$ suggests an extensional flow; and finally, a negative case ($G = -1$), where the fluid rotates clockwise.

The undisturbed motion with a positive nonlinear intensity ($E = 1$) is described in figure 3. The case $G = \infty$ is similar to the linear flow in the y-direction of figure 2, since then the linear velocity term is much larger than the nonlinear term. The remaining three cases are all similar in form, with the case $G = -1$ also showing a clockwise circulation. This circulation increases in size as E decreases, until the image of the linear case ($G = -1$, $E = 0$) is recovered.

Probably the most interesting undisturbed motion case is shown in figure 4, where the nonlinear intensity of the flow is negative ($E = -1$). Once again, the case $G = \infty$ is similar to the linear flow in the y-direction of figure 2, since then the linear velocity term is much larger than the nonlinear term. The third case ($G = 1$) is fascinating, since, if observing it from an angle of $\phi = \pm 45°$, it mimics a drop in an extensional flow, with the familiar internal circulations, despite the fact that there is no drop at all! Figures 2–4 show just a few possibilities for the undisturbed motion. Many more interesting streamline shapes can be obtained by exploring different combinations of G and E, as a result of the inclusion of nonlinear terms to the velocity field, which among other features, also suggests up to eight stagnation points, besides the one at the origin which always is present. These are located at: $(0, 0)$; $(0, \pm i/\sqrt{E})$; $(\pm i\sqrt{G/E}, 0)$; $(\pm i\sqrt{G/E}, \pm i/\sqrt{E})$; and $(\pm i\sqrt{G/E}, \mp i/\sqrt{E})$.

https://doi.org/10.1017/jfm.2022.309 Published online by Cambridge University Press

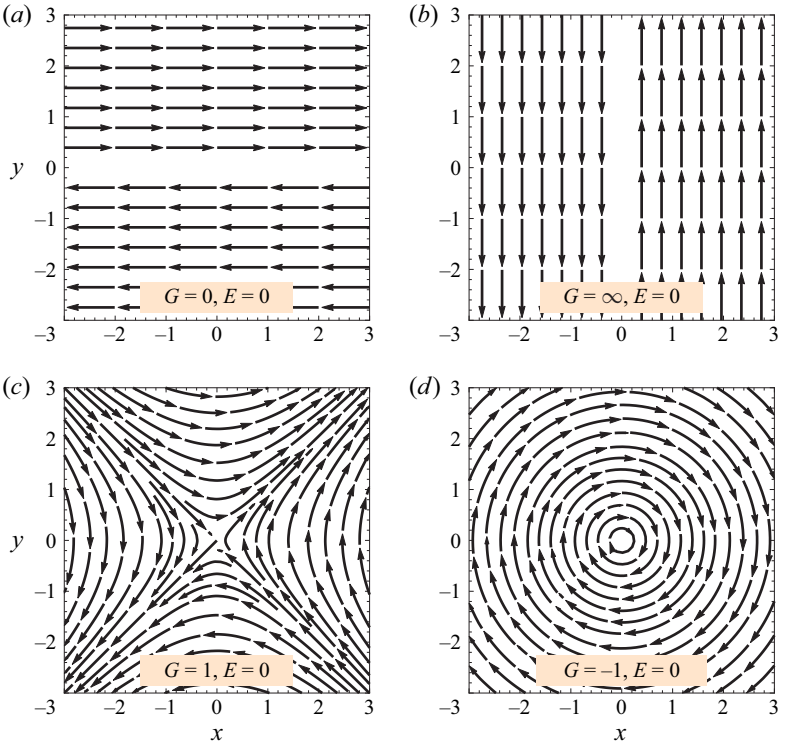


Figure 2. The undisturbed motion in a linear ($E=0$) shear flow.

4. The disturbed motion

The flow in the presence of a spherical drop, corresponding to the limit of $Ca=0$, can be obtained by solving the Stokes equations with the appropriate boundary conditions, as suggested by (2.13)–(2.27). It appears that, if the linear case ($E=0$) can be satisfied with $n=1$ and 2, our nonlinear problem requires $n=1$, 2, 3 and 4. With the assistance of the Mathematica software, the following analytical expressions for the coefficients in the solid harmonics were obtained. For the external flow we have

$$b_{-3,2} = -\frac{(2+5\lambda)(1+G)}{6(1+\lambda)} - \frac{\lambda E}{(1+\lambda)}, \tag{4.1}$$

$$b_{-5,2} = +\frac{(2+9\lambda)E}{75(1+\lambda)}, \tag{4.2}$$

$$d_{-3,2} = -\frac{\lambda(1+G)}{12(1+\lambda)} + \frac{(2-5\lambda)E}{42(1+\lambda)}, \tag{4.3}$$

$$d_{-5,2} = +\frac{\lambda E}{150(1+\lambda)}, \tag{4.4}$$

$$e_{-4,2} = +\frac{(1-\lambda)E}{30(5+2\lambda)}. \tag{4.5}$$

https://doi.org/10.1017/jfm.2022.309 Published online by Cambridge University Press

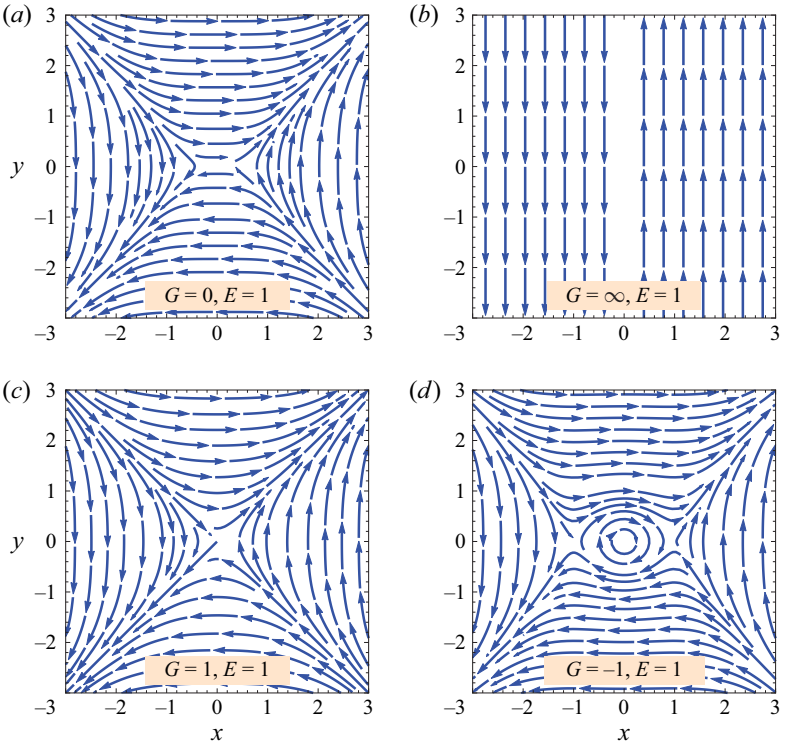


Figure 3. The undisturbed motion in a positive nonlinear ($E > 0$) shear flow.

While the coefficients of the internal flow are

$$b_{2,2} = +\frac{7\lambda(1+G)}{4(1+\lambda)} + \frac{7\lambda E}{2(1+\lambda)}, \tag{4.6}$$

$$b_{4,2} = -\frac{11\lambda E}{60(1+\lambda)}, \tag{4.7}$$

$$d_{2,2} = -\frac{(1+G)}{8(1+\lambda)} - \frac{E}{4(1+\lambda)}, \tag{4.8}$$

$$d_{4,2} = +\frac{E}{120(1+\lambda)}, \tag{4.9}$$

$$e_{1,0} = -\frac{(1-G)}{2}, \tag{4.10}$$

$$e_{3,2} = +\frac{7E}{60(5+2\lambda)}, \tag{4.11}$$

where the rest of the coefficients vanish.

Figure 5 represents the velocity vector of the disturbed motion, in the $z = 0$ plane, for the familiar simple (linear) shear flow ($E = 0$, $G = 0$), where the velocity of the unperturbed motion is in the x-direction only. This case has been extensively explored by Bartok & Mason (1958). Four viscosity ratios are presented, from a bubble or an inviscid drop ($\lambda = 0$) up to a solid sphere ($\lambda = \infty$). When $\lambda = 0$, the external streamlines are open while the internal streamlines suggest the familiar '8' shape combined with

https://doi.org/10.1017/jfm.2022.309 Published online by Cambridge University Press

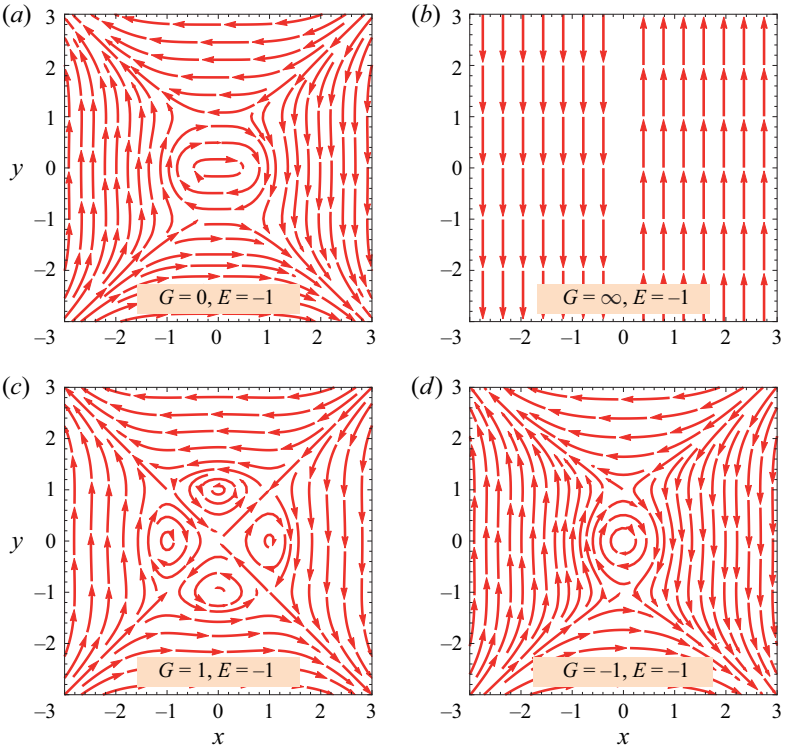


Figure 4. The undisturbed motion in a negative nonlinear ($E < 0$) shear flow.

oval streamlines. A similar picture is observed for the $\lambda = 0.1$ case, except that the external streamlines are closed. For low values of λ, where the '8' shape exists, the drop contains two additional stagnation points, besides the one at the origin. At $z = 0$, these are located at $\phi = 90°$ and $\phi = 270°$ and at $r = \sqrt{(1 - 2\lambda)/5}$ suggesting that the '8' shape can be established only if $\lambda < 1/2$ (Bartok & Mason 1958). Next is $\lambda = 1$, where the two phases are of equal viscosity, and where the internal streamlines are everywhere oval in shape. Finally, when $\lambda = \infty$, the drop becomes a solid sphere rotating clockwise at an angular velocity $\omega = -1/2$ in accordance with the literature. In general, the angular velocity of a solid sphere in this problem is $\omega = -(1 - G)/2$ and independent of E.

Another interesting feature of the flow field is the location of surface stagnation points. At the surface of the drop ($r = 1$) and at the $z = 0$ plane ($\eta = 0$), $v_r = v_\theta = 0$, and the condition for a vanishing v_ϕ leading to a stagnation point can be expressed as

$$\phi = \pm\frac{1}{2}\cos^{-1}\left[\frac{10(1-G)(1+\lambda)(5+2\lambda)}{10(1+G)(5+2\lambda)+7E(20+11\lambda)}\right] + n\pi, \tag{4.12}$$

where n is an integer. It follows that, for the cases described in figure 5 ($G = E = 0$), only the inviscid drop ($\lambda = 0$) predicts real azimuthal angles which are located at $\phi = 0°$ and $\phi = 180°$. The inviscid drop is also the only case in figure 5 suggesting no closed external streamlines, an important issue when dealing with mass transfer problems around such a drop.

Next, in figure 6, we continue with the velocity vector in a linear shear flow ($E = 0$) at the $z = 0$ plane, but with a positive linear velocity ratio ($G > 0$). Two viscosity ratios ($\lambda = 0$, 1) and two linear velocity ratios ($G = 1$, 10) are described. For the two $G = 1$ cases, and if

https://doi.org/10.1017/jfm.2022.309 Published online by Cambridge University Press

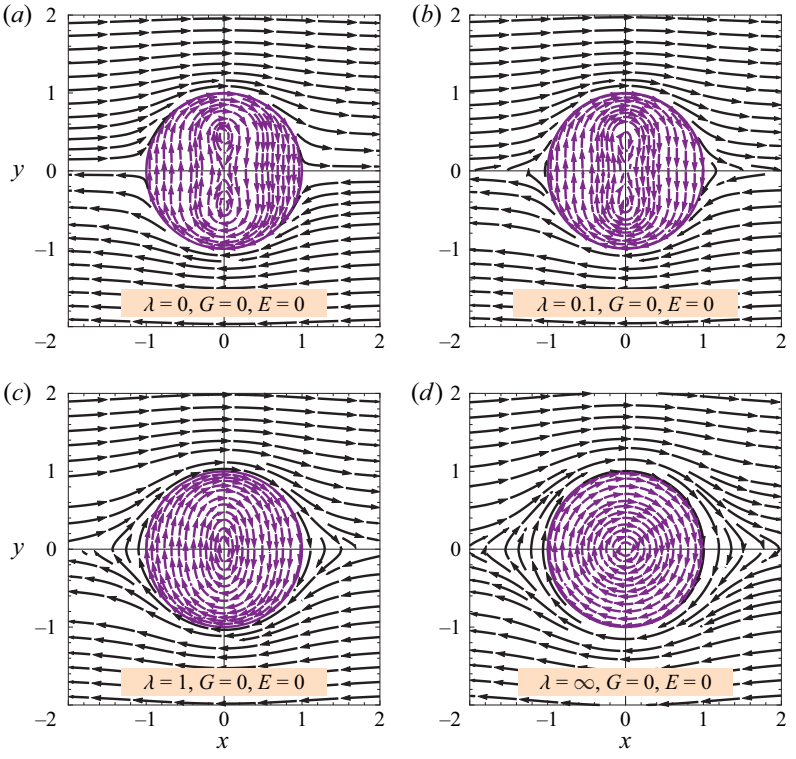


Figure 5. The disturbed motion in a linear ($E=0$) shear flow, with $G=0$, as a function of λ.

observing at $\phi=\pm45°$, an extensional flow is produced (see figure 2, $G=1$) suggesting similar streamlines shapes for all values of λ. However, when $G\gg1$, the external flow moves towards a simple shear flow in the in the y-direction (see figure 2, $G=\infty$), where, similar to the familiar simple shear flow (figure 5), the shape of the internal streamlines strongly depends on λ. The surface stagnation points in figure 6 can be easily located according to (4.12). The case $G=1$ is unique since it suggests the simple expression of $\phi=(\pm1/4+n)\pi$, which is independent of λ or E. The angular velocity of a solid sphere ($\lambda=\infty$) is $\omega=-(1-G)/2$ and independent of E. That is, for $G=1$ it vanishes, while for $G>1$ it results in $\omega>0$ or a counter-clockwise rotation.

Figures 5 and 6 suggests that, for the linear case ($E=0$), the internal flow within the drop contains zero, two or four stagnation points, besides the one at the origin. The first pair is located at $\phi=0°$ and $\phi=180°$, and its distance from the origin is

$$r=\sqrt{\frac{5+2\lambda+(1-2\lambda)G}{5(1+G)}}. \tag{4.13}$$

While the next pair is positioned at $\phi=90°$ and $\phi=270°$, and at

$$r=\sqrt{\frac{1-2\lambda+(5+2\lambda)G}{5(1+G)}}. \tag{4.14}$$

It follows that, for $G=1$, these two pairs are at equal distance $r=\sqrt{3/5}=0.775$ from the origin and independent of λ. When $\lambda=0$ and $G=10$, the first pair is at

https://doi.org/10.1017/jfm.2022.309 Published online by Cambridge University Press

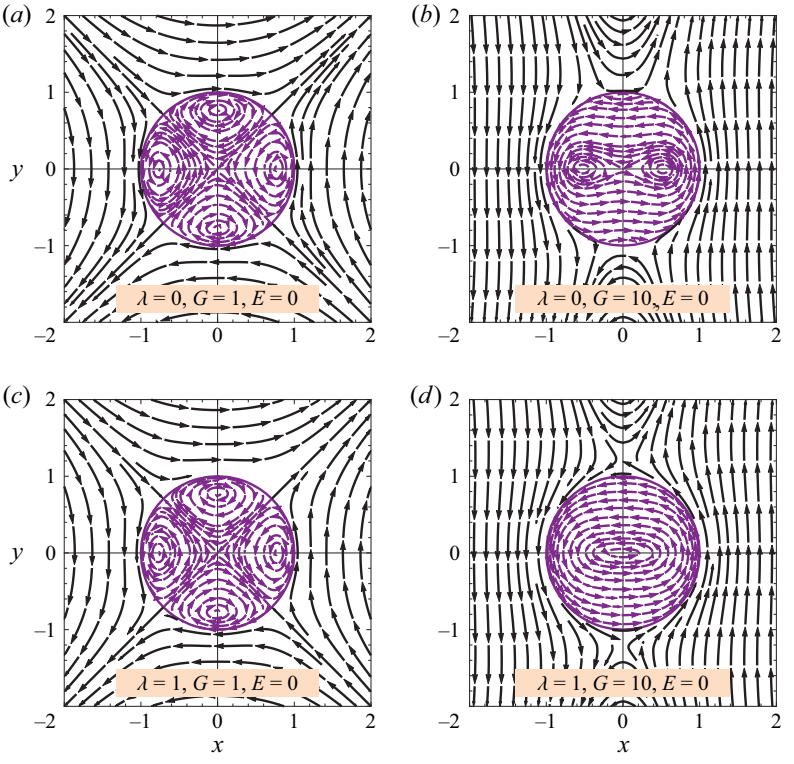


Figure 6. The disturbed motion in a linear ($E=0$) shear flow, with $G>0$, as a function λ.

$r=\sqrt{3/11}=0.522$, and the second one at $r=\sqrt{51/55}=0.963$. However, if $\lambda=1$ and $G=10$, the first pair does not exist (r is imaginary), and the second one does not exist either ($r>1$).

Figure 7 finalizes our linear ($E=0$) findings, by plotting the velocity vector at the $z=0$ plane, with a negative velocity ratio ($G<0$). As in figure 6, two viscosity ratios ($\lambda=0,\ 1$) and two linear velocity ratios ($G=-1,\ -10$) are presented. The case $E=0$ and $G=-1$ is unique since, in the entire space, all velocity components vanish except $v_{\phi in}=v_{\phi out}=-r\sin\theta$, independent of λ. That is, the drop rotates clockwise like a solid particle at an angular velocity $\omega=-1$. As G becomes more negative, the external streamlines change their configuration from circles towards ellipse-like shapes and, if $|G|\gg 1$, we approach a simple shear flow in the y-direction but in opposite direction to the one presented in figure 2. When $G<0$ ($E=0$), (4.12) predicts no stagnation points at the surface of the drop. Figure 7 shows that, if $G<0$ ($G\neq -1$), the internal circulation is a strong function of λ, predicting once again oval shape streamlines with or without the '8' structure (which now lies down). The internal stagnation points, besides the one at the origin, can be obtained from (4.13) and (4.14), where it is clear that, if $G=-1$, they do not exist as the denominator vanishes. For the $G=-10$ cases described here, only $\lambda=0$ predicts internal stagnation points and only one pair located at $\phi=0°$ and $\phi=180°$ at a distance $r=1/3$ from the origin.

Now that we are familiar with the disturbed linear ($E=0$) behaviour, we can move forward and explore nonlinear ($E\neq 0$) shear flows in the presence of a drop. For a spherical drop ($Ca=0$), the problem is governed by three dimensionless numbers (λ, G, E), and the

https://doi.org/10.1017/jfm.2022.309 Published online by Cambridge University Press

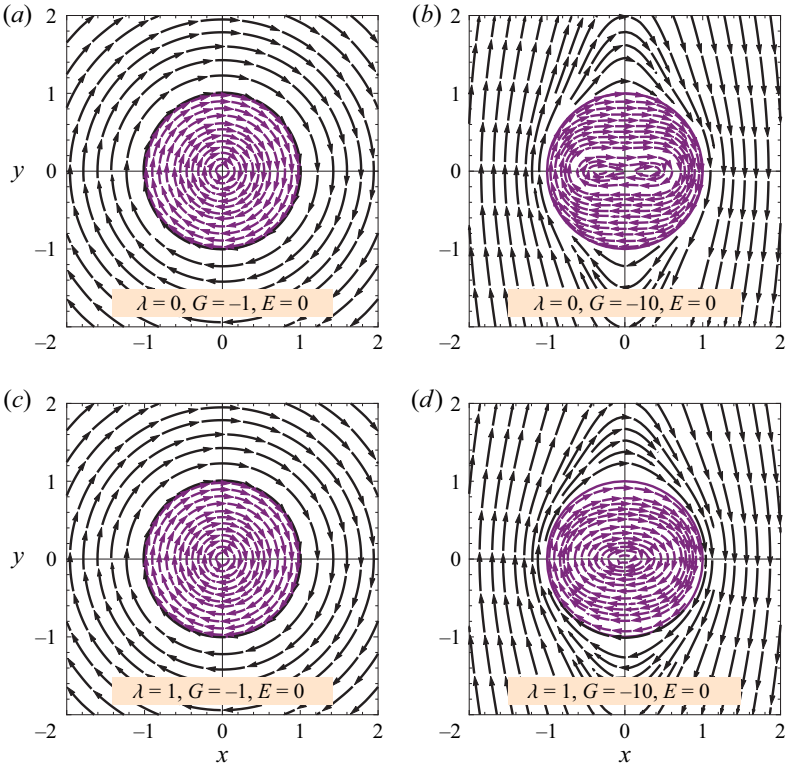


Figure 7. The disturbed motion in a linear ($E=0$) shear flow, with $G<0$, as a function λ.

number of combinations is extremely large. To reduce the number of figures, we explore the case $\lambda=1$ only, at three different linear velocity ratios ($G=0$, 1, -1). All forthcoming velocity vector plots are shown at the $z=0$ plane.

The first nonlinear plot of the disturbed motion is presented in figure 8, where $\lambda=1$, $G=0$ and E adopts positive and negative values. In the first case ($E=0.1$), the nonlinear intensity of the flow is weak, and since $G=0$, the flow behaviour is not far from the familiar simple shear flow ($G=0$, $E=0$). Some differences are observed in the external flow, where the present case has stagnation points at $\phi=0°$, $\phi=180°$ and $r=1.15$, whereas the linear case has not. On the other hand, the internal streamlines are oval, with no stagnation points apart from the origin, as in the familiar simple shear flow case $\lambda=1$. No stagnation points are present at the surface of the drop. Next, we increase the nonlinear intensity ($E=1$) and dramatic changes occur everywhere. Now, the external flow does not contain stagnation points, but the surface of the drop does ($\phi=\pm30.4°$, $\pm149.6°$). Inside the drop, four additional stagnation points are created, at the usual azimuthal angles. The first pair is located at $\phi=0°$ and 180° with $r=0.874$, while for the second one we have $\phi=90°$ and 270° with $r=0.547$.

When $E<0$, and if $G=0$, the undisturbed motion has stagnation points (besides the origin) at $x=0$, $y=\pm i/\sqrt{E}$. As $|E|$ increases and the flow becomes more nonlinear, this stagnation point moves towards the origin. For $E=-1/2$, this point is located at $(0,\pm\sqrt{2})$ and its location, if the flow is disturbed, is not far away from it $(0,\pm1.39)$. The direction of the flow above and below of this point is reversed, as can be seen in the first $E<0$ case of figure 8. No stagnation points are predicted at the surface of the drop or inside the

https://doi.org/10.1017/jfm.2022.309 Published online by Cambridge University Press

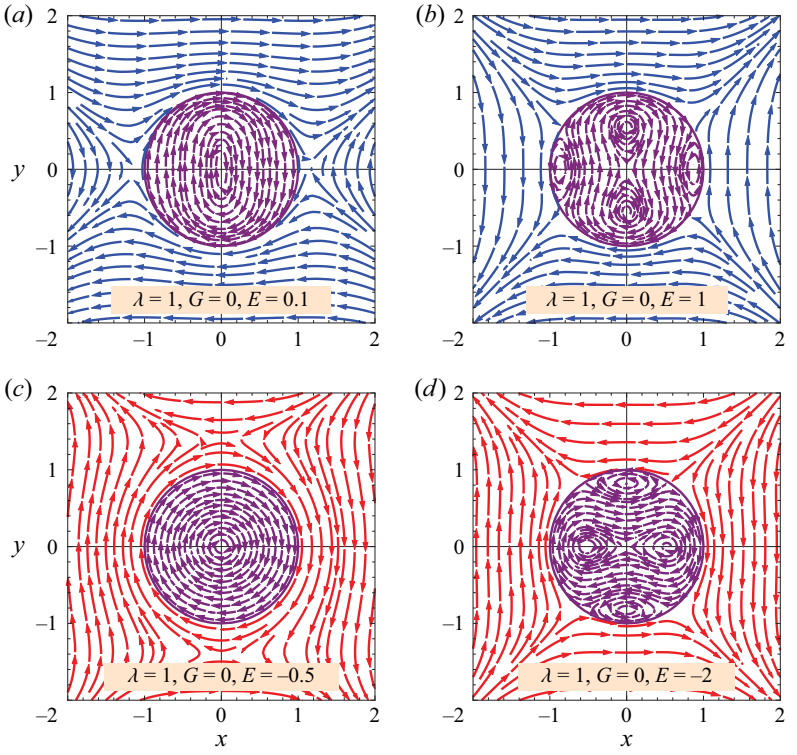


Figure 8. The disturbed motion in a nonlinear ($E \neq 0$) shear flow, with $\lambda = 1$ and $G = 0$, as a function of E. Blue: $E > 0$; red $E < 0$.

drop, except at the origin. As $|E|$ continues to increase, $\pm i/\sqrt{E}$ approaches the origin, and the stagnation point in the external fluid, where the flow changes direction, does not exist anymore. This is illustrated in the last example of figure 8 where four stagnation points are created at the surface of the drop ($\phi = \pm 56.3°, \pm 123.7°$) and four others within the drop ($\phi = 0°$, 180° and $r = 0.522$; $\phi = 90°$, 270° and $r = 0.828$).

The next nonlinear disturbed motion plot is shown in figure 9, where $\lambda = 1$ and $G = 1$ for all cases. The two positive nonlinear intensities $E = 1$ and $E = 10$, are not only similar in form, but they also behave as in the linear case ($\lambda = 1$, $G = 1$, $E = 0$) in figure 6. That is, if observing from an angle $\phi = \pm 45°$, we have an extensional flow. The only difference between the cases is the volumetric flow rate which increases with an increase in E. Stagnation points are not present in the external flow; however, they are present at the surface of the drop ($\phi = \pm 45°, \pm 135°$), and within the drop ($\phi = 0°, 90°, 180°, 270°$). It appears that, for a constant λ and if $G = 1$, all these four points are located at equal distances from the origin. For $\lambda = 1$ we have: $E = 0$, $r = \sqrt{3/5} = 0.775$; $E = 1$, $r = 0.741$; $E = 10$, $r = 0.716$; $E = \infty$, $r = 0.711$. Thus, the distance of the internal stagnation points from the origin slightly decreases as E increases.

The two cases at the bottom of figure 9 correspond to $\lambda = 1$, $G = 1$ and $E < 0$. Since both $E < 0$ and $G/E < 0$, the undisturbed motion predicts eight stagnation points besides the one at the origin. These are located at: $(0, \pm i/\sqrt{E})$; $(\pm i\sqrt{G/E}, 0)$; $(\pm i\sqrt{G/E}, \pm i/\sqrt{E})$; and $(\pm i\sqrt{G/E}, \mp i/\sqrt{E})$. The stagnation points move towards the origin as $|E|$ increases. In the first case, $G = 1$ and $E = -1/2$, the first two pairs are located at $(0, \pm\sqrt{2})$ and $(\pm\sqrt{2}, 0)$ and

https://doi.org/10.1017/jfm.2022.309 Published online by Cambridge University Press

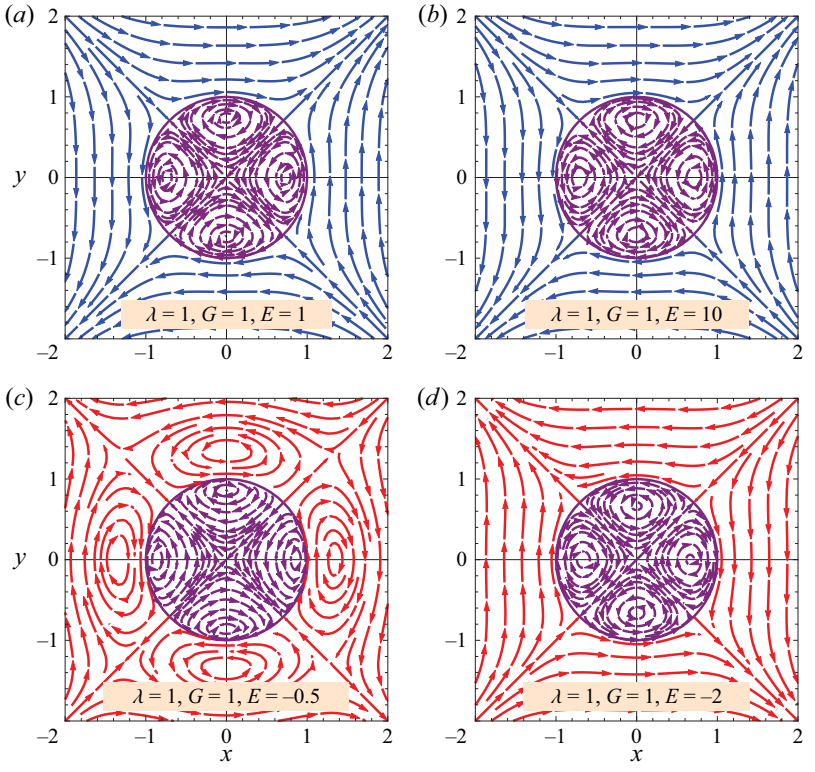


Figure 9. The disturbed motion in a nonlinear ($E \neq 0$) shear flow, with $\lambda = 1$ and $G = 1$, as a function of E. Blue: $E > 0$; red $E < 0$.

their position in the disturbed motion is not far from (0, ± 1.35) and (± 1.35, 0). Around these stagnation points, circulations are formed. In addition, four stagnation points in the external fluid can be observed at ($\phi = \pm 45°$, $\pm 135°$, $r = 1.78$) to support such complex structure. As $|E|$ increases and the flow becomes more nonlinear, as can be seen in the last example of figure 9 ($E = -2$), these eight stagnation points just described move towards the origin and disappear in the external fluid. Both $E < 0$ cases suggest four stagnation points at the surface of the drop ($\phi = \pm 45°$, $\pm 135°$, $r = 1$), and another four (besides the origin) within the drop ($\phi = 0°$, 90°, 180°, 270°). Those within the drop move toward the surface as $|E|$ increases from $E = 0$ ($E = 0$, $r = \sqrt{3/5} = 0.775$; $E = -0.5$, $r = 0.867$; $E = -0.645$, $r = 0.9997$). These points disappear in the range $-1 < E < -0.646$, and emerge once again at $E < -1$ ($E = -1$, $r = 0$; $E = -2$, $r = 0.664$; $E = -10$, $r = 0.706$; $E = -\infty$, $r = 0.711$).

The last undisturbed motion is presented in figure 10, where once again $\lambda = 1$ but with a negative linear velocity ratio ($G < 0$). The first positive nonlinear intensity case ($E = 1$) should be compared with its equivalent undisturbed motion in figure 3 ($G = -1$, $E = 1$). The external fluid contains two stagnation points ($\phi = 0°$, 180°, $r = 1.07$); however, the surface of the drop and the internal fluid (except the origin) do not. As E increases, as shown in the second case ($E = 5$), the stagnation points in the external fluid disappear, yet they emerge at the surface of the drop ($\phi = \pm 37.5°$, $\pm 142.5°$) and within the drop ($\phi = 0°$, 180° and $r = 0.798$; $\phi = 90°$, 270° and $r = 0.612$). For $\lambda = 1$ and $G = -1$, the first pair ($\phi = 0°$, 180°) appears if $E > 1.29$ from $r = 1$ and reaches $r = 0.711$ at $E = \infty$, while

https://doi.org/10.1017/jfm.2022.309 Published online by Cambridge University Press

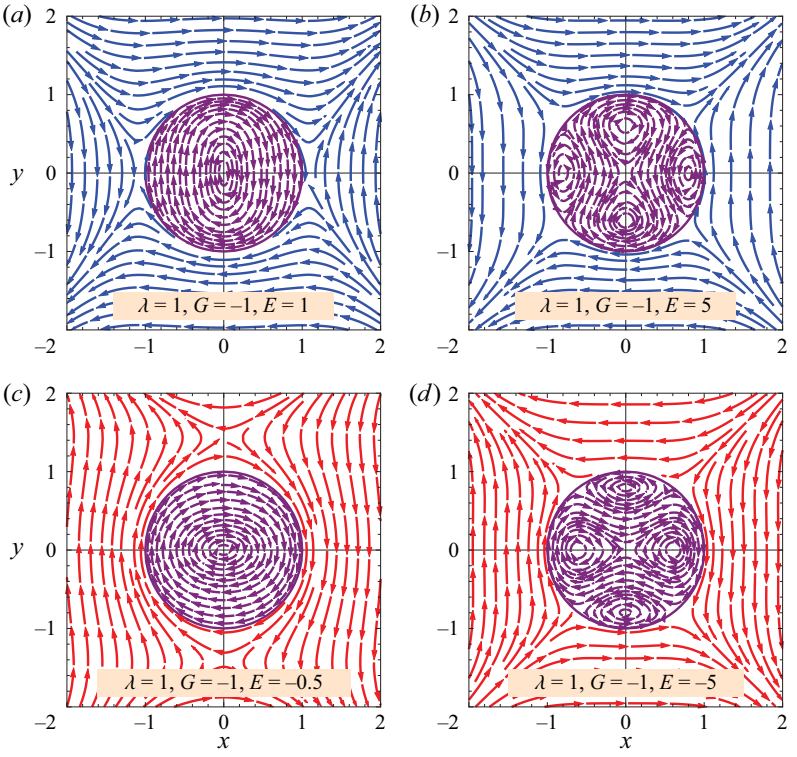


Figure 10. The disturbed motion in a nonlinear ($E \neq 0$) shear flow, with $\lambda = 1$ and $G = -1$, as a function of E. Blue: $E > 0$; red $E < 0$.

the second pair ($\phi = 90°$, 270°) appears when $E > 1.33$ from $r = 0$ and approaches also $r = 0.711$ at $E = \infty$.

The next two cases correspond to negative nonlinear intensities ($E < 0$). In the first one ($E = -0.5$), the external flow contains two stagnation points ($\phi = 90°$, 270°, $r = 1.43$), not far from those of the undisturbed motion $(0, \pm\sqrt{2})$. Yet, both the surface of the drop and the internal fluid (besides the origin) do not contain stagnation points. As $|E|$ increases and the flow becomes more nonlinear ($E = -5$), the situation is reversed. Stagnation points in the external fluid disappear, but appear at the surface ($\phi = \pm 52.5°$, $\pm 127.5°$) and within the drop ($\phi = 0°$, 180° and $r = 0.612$; $\phi = 90°$, 270° and $r = 0.798$). For $\lambda = 1$ and $G = -1$, the first pair ($\phi = 0°$, 180°) appears if $E < -1.33$ from $r = 0$ until $r = 0.711$ at $E = -\infty$, while the second pair ($\phi = 90°$, 270°) appears if $E < -1.29$ from $r = 1$ and approaches $r = 0.711$ at $E = -\infty$. Thus, one concludes that, if the present situation ($E = -5$) is rotated at $\phi = 90°$, the previous internal findings ($E = 5$) are recovered.

5. Deformation of the drop

So far, the velocity profiles outside and inside a spherical drop, representing the $O(Ca^0)$ solution, are available to us. The normal viscous stresses can be evaluated from Newton's viscosity law, and the pressures from (2.14) and (2.19). These can be then substituted into the normal stress balance, (2.28), that has not been applied yet, to obtain the $O(Ca^1)$ shape of the deformed drop. Let the distance from the origin to the surface of the deformed drop

https://doi.org/10.1017/jfm.2022.309 Published online by Cambridge University Press

be

$$R(\theta, \phi) = 1 + Caf(\theta, \phi), \tag{5.1}$$

Where, according to Landau & Lifshitz (1987), the shape function $f(\theta, \phi)$ is connected to the principal radii of curvature, obtained from the normal stress balance, as follows:

$$\frac{1}{R_1} + \frac{1}{R_2} = 2 - Ca(2f + \nabla^2 f). \tag{5.2}$$

In (5.2), the Laplacian operator should be in spherical coordinates. After some algebraic manipulation, the expression the shape of the deformed drop is given by

$$R = 1 + Ca(1 + G)\frac{(16 + 19\lambda)}{16(1 + \lambda)}(1 - \eta^2)\sin(2\phi) + CaE\frac{7[28 + 41\lambda - \eta^2(16 + 17\lambda)]}{240(1 + \lambda)}(1 - \eta^2)\sin(2\phi). \tag{5.3}$$

When $G = E = 0$, the shape of the familiar (linear) simple shear flow is recovered. The maximum and minimum semi-axes in the $z = 0$ ($\eta = 0$) plane can be found by solving $\partial R/\partial\phi = 0$. As expected, these are located at the principal axes of extension or compression ($\phi = \pm 45°, \pm 135°$), for both linear and nonlinear shear flows. The expression presented here for the shape of the drop is valid for a slightly deformed drop with $\lambda = O(1)$, $G = O(1)$, $E = O(1)$ and $Ca \ll 1$. For a simple shear flow, Taylor (1934) showed that small deformations are also possible for highly viscous drops $\lambda \gg 1$ with $Ca = O(1)$ where the major axis of the deformed drop is positioned in the direction of the flow. In section 6 we shall discuss high viscosity drops.

Figure 11 describes the shape of a drop with $\lambda = 1$ and $G = 0$ at different values of Ca. Each figure contains the linear case ($E = 0$) as well as positive and negative nonlinear intensities ($E = \pm 1$). As expected, the deformation of the drop increases as Ca increases. When the nonlinear intensity is positive ($E = 1$), the drop is more elongated than the linear case, and when it is negative ($E = -1$), the drop is less elongated than the linear case. This is also expressed by the familiar centre pinching or peanut shape, which for $E > 0$ it is developed at a lower Ca than the linear case, and for $E < 0$ it is not developed at all as a result of extremely small deformations. At $\phi = 0°$, 90°, 180° and 270°, the distance of the surface to the origin is $R = 1$.

In figure 12 we continue to describe the shape of the same drop ($\lambda = 1$), but this time the linear velocity ratio is $G = 1$. Once again, each figure accommodates three different nonlinear intensities ($E = 0, \pm 1$). It appears that the same behaviour observed in the previous case ($G = 0$) occurs here ($G = 1$) as well. That is, the deformation of the drop increases with an increase in E. Note that the influence of G on the shape of the drop takes place only in the second (linear) term on the right-hand side of (5.3). It is clear from the shape expression that larger deformations are to be expected when $G = 1$ (figure 12) than when $G = 0$ (figure 11). This is also reflected by the evidence that, contrary to figure 11, this time even the $E = -1$ case shows the peanut shape. The last case had to be stopped at $Ca = 0.313$ as, beyond that, no steady shape was possible for $E = 1$.

Finally, in figure 13 we portray the deformation of the drop when $\lambda = 1$ and $G = -1$. The case $G = -1$ is unique since the second (linear) term on the right-hand side of the shape (5.3) vanishes. Furthermore, for the linear case ($E = 0$), even the last term on the right-hand side vanishes, suggesting that no deformation is possible since the unperturbed flow contains vorticity but not angular deformation. The two nonlinear situations of $E = \pm 1$ offer the same deformation but at different orientations. For $E = 1$, the drop is aligned

https://doi.org/10.1017/jfm.2022.309 Published online by Cambridge University Press

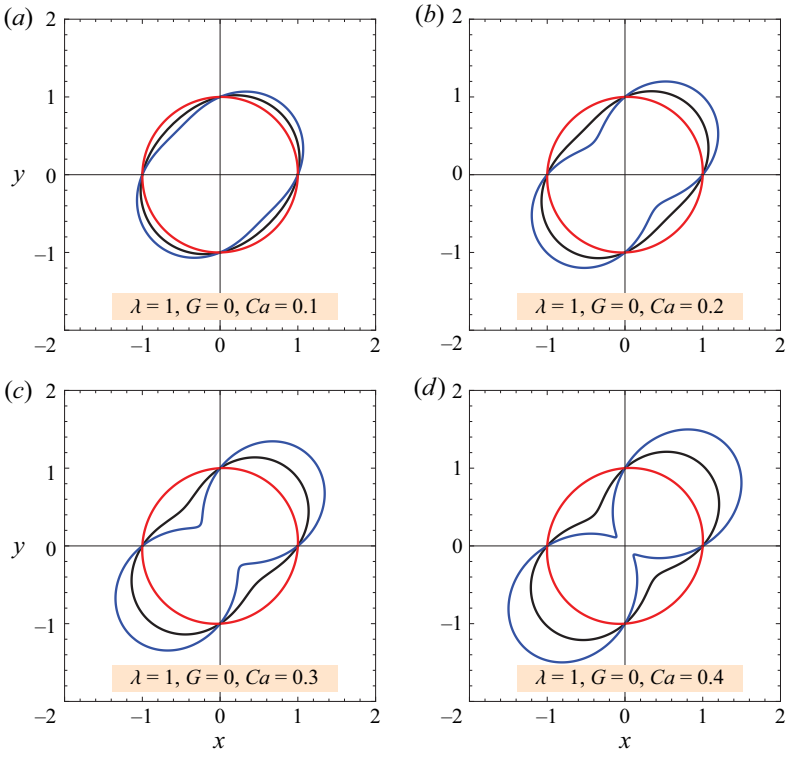


Figure 11. The shape of a drop with $\lambda = 1$ and $G = 0$ as a function of Ca. Black: $E = 0$; blue: $E = 1$; red $E = -1$.

at $\phi = 45°$, while for $E = -1$ at $\phi = -45°$; however, it is possible to orient the drop at $\phi = \pm 45°$ for all cases of E (zero, positive or negative). When $G < 0$ and if $|G|$ is relatively large, an opposite picture than figures 11 and 12 is obtained. That is, all drops are aligned at $\phi = -45°$, if $E < 0$, the drop is more elongated than the linear case, and if $E > 0$ it is less elongated than the linear case.

Figures 11–13 confirmed that the drop sometimes is aligned at $\phi = 45°$ and sometimes at $\phi = -45°$, that is, in the principal directions of elongation. When the drop shifts from one orientation to the other it passes via the spherical shape where no deformation is taking place, even at $Ca \neq 0$. This combination of parameters can be anticipated by letting $R = 1$ in (5.3)

$$G = -\left[1 + \frac{7(28 + 41\lambda)}{3(80 + 95\lambda)}E\right]. \tag{5.4}$$

Thus, taking the examples in figures 11–13 ($\lambda = 1$), this shift occurs at: $G = -1$ ($E = 0$, shown in figure 13), $G = -48/25 = -1.92$ ($E = 1$) and $G = -2/25 = -0.08$ ($E = -1$).

As noticed in figures 11–13, at larger capillary number, the drop adopts a peanut shape similar in appearance to the case of a centre pinching breakup mechanism. So, it would be interesting to determine the critical capillary number at which the physical drop shape ceases to exist. Of course, this cannot be considered as the official breakup point since drop breakup is a transient unstable situation which the steady and slightly perturbed sphere approximation performed here cannot predict. Nevertheless, we feel that this limit is valuable to the analysis presented here. Substituting $R = 0$ at $\phi = \pm 45°$ in (5.3), we find

https://doi.org/10.1017/jfm.2022.309 Published online by Cambridge University Press

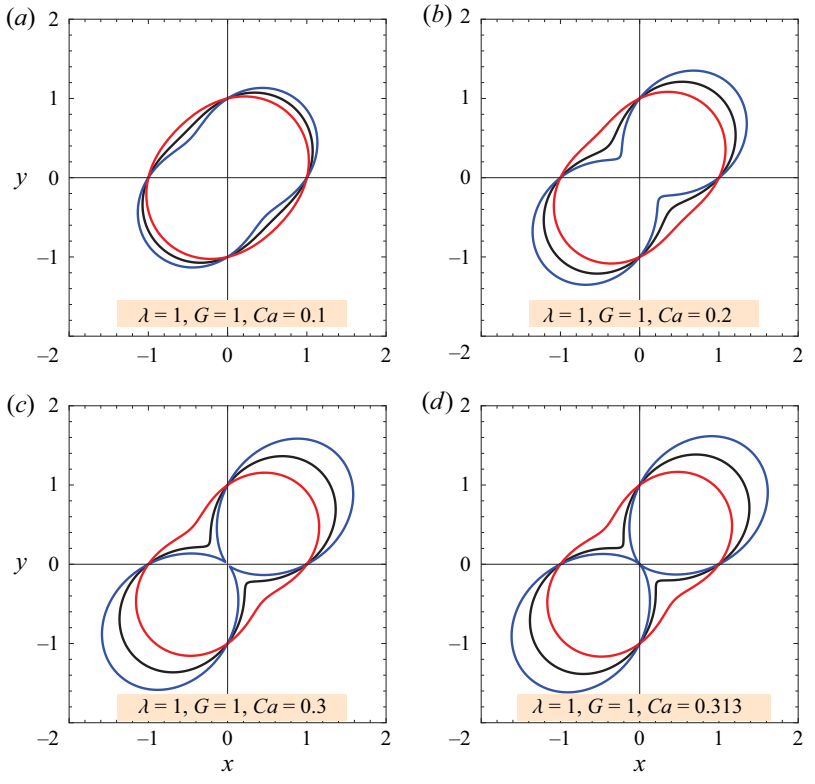


Figure 12. The shape of a drop with $\lambda = 1$ and $G = 1$ as a function of Ca. Black: $E = 0$; blue: $E = 1$; red $E = -1$.

this critical value to be

$$Ca_{cr} = \frac{240(1+\lambda)}{15(1+G)(16+19\lambda)+7E(28+41\lambda)}. \tag{5.5}$$

Thus, taking the example of figure 12 ($\lambda = 1$, $G = 1$), this occurs at: $Ca_{cr} = 16/35 = 0.457$ ($E = 0$), $Ca_{cr} = 160/511 = 0.313$ ($E = 1$, shown in figure 12) and $Ca_{cr} = 160/189 = 0.847$ ($E = -1$).

In the drop deformation literature, it is common to introduce the Taylor deformation parameter (Taylor 1934) as a measure of the deformation magnitude. Let $L = R_{max}$ and $B = R_{min}$ be the major and minor radii of the drop. Applying a Taylor series on Taylor's deformation parameter for Ca, around $Ca = 0$, results in

$$D = \frac{L-B}{L+B} = \left| \frac{(16+19\lambda)}{16(1+\lambda)}(1+G)Ca + \frac{7(28+41\lambda)}{240(1+\lambda)}Ca\,E \right|, \tag{5.6}$$

where $D = 0$ suggests a sphere and $D \to 1$ denotes a slender drop. Note that we included the absolute value, as we already saw that sometimes the major radius is at $\phi = 45°$ and sometimes at $\phi = -45°$. Figure 14 describes the Taylor deformation parameter as a function of the capillary number (Ca), the viscosity ratio (λ), the linear velocity ratio (G) and the nonlinear intensity of the flow (E). The first case ($G = 0$), confirms once again our finding of figure 11 ($G = 0$) that, for the same Ca, when $E > 0$, the drop is more elongated than the linear case ($E = 0$), and when $E < 0$ the drop is less elongated than the linear case.

https://doi.org/10.1017/jfm.2022.309 Published online by Cambridge University Press

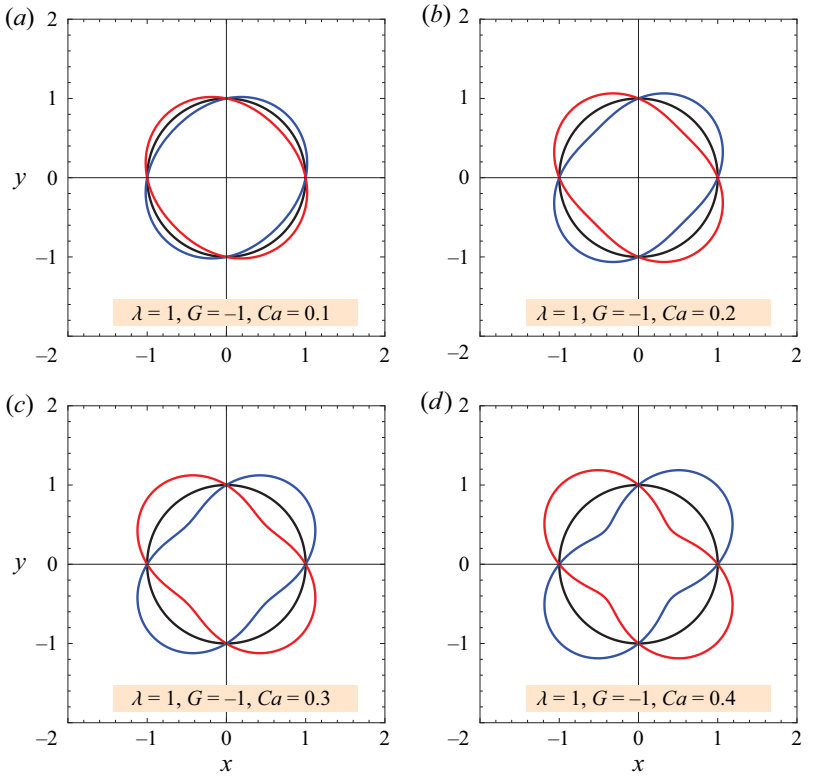


Figure 13. The shape of a drop with $\lambda = 1$ and $G = -1$ as a function of Ca. Black: $E = 0$; blue: $E = 1$; red $E = -1$.

Furthermore, when $E \geq 0$, as λ increases the drop is more elongated; however, when $E < 0$ the opposite is expected. The next case ($G = 1$), see also figure 12, repeats the $G = 0$ trends, but with a larger deformation. Here, the λ influence is practically indistinguishable for $E = -1$. The last two cases correspond to $G < 0$, where the example of figure 13 ($G = -1$) was not selected as it predicts no deformation for the linear case, and equal deformation (but not orientation) at $E = \pm 1$. When $G = -0.5$, once again, if $E > 0$, the drop is more elongated than the linear case and if $E < 0$ the drop is less elongated than the linear case. Also, as λ increases the drop is more elongated for all E cases. In the last situation, where $G = -2$, the major radius in all E cases is oriented at $\phi = -45°$, and the deformation of the drop increases as E decreases. Moreover, when $E \leq 0$ the elongation increases as λ increases, and the opposite occurs at $E > 0$. To summarize, the Taylor deformation parameter is primarily affected by G and E, while λ variations are of second importance.

6. Deformation of a very viscous drop

Taylor (1934) also treated the case of a very viscous drop ($\lambda \gg 1$), where the shape of the drop remains almost spherical, even at $Ca = O(1)$. This is possible when the external flow has sufficient vorticity (such as in simple shear flow) resulting in the high viscosity drop rotating almost as if it were a solid particle (Frankel & Acrivos 1970; Stone 1994). Accordingly, we repeat Taylor's solution procedure, as follows. The normal stress balance, (2.28), with the right-hand side equal to $2/Ca$, is included, the normal velocities are

https://doi.org/10.1017/jfm.2022.309 Published online by Cambridge University Press

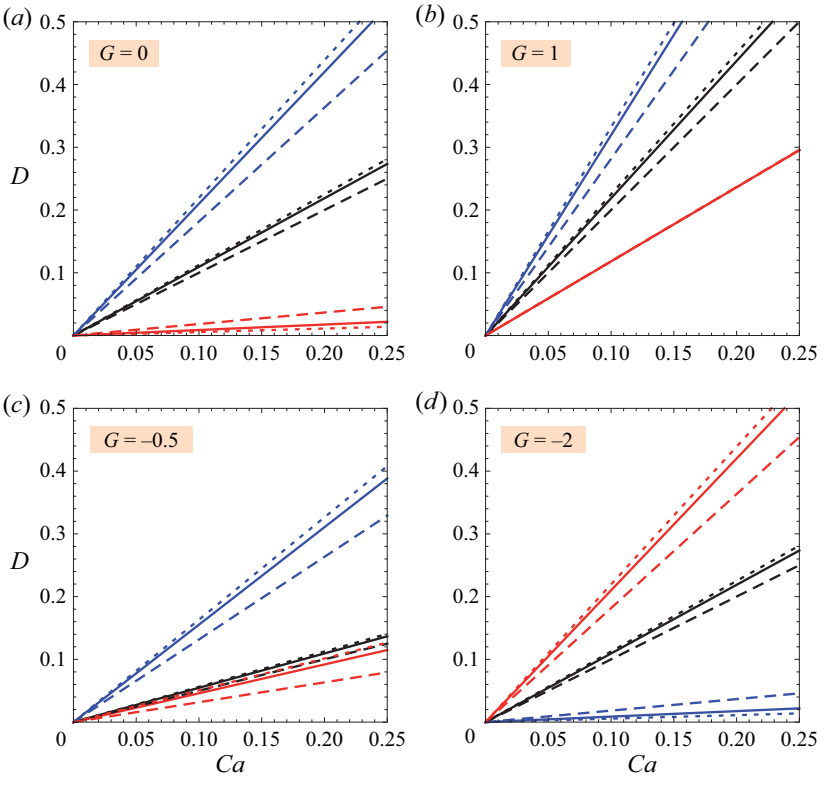


Figure 14. The Taylor deformation parameter, as a function of Ca, for different values of λ, G and E. Black, $E=0$; blue, $E=1$; red, $E=-1$. Solid lines, $\lambda=1$; dashed lines, $\lambda=0$; dotted lines, $\lambda=2$.

still continuous; however, they do not vanish. Once again, with the assistance of the Mathematica software, an analytical solution of $O(Ca^0)$ has been obtained. For the external flow, the coefficients of the solid spherical harmonics are now

$$b_{-3,2} = +\frac{5(1-\lambda)(1+G)}{3(3+2\lambda)} + \frac{2(1-\lambda)E}{(3+2\lambda)}, \tag{6.1}$$

$$b_{-5,2} = -\frac{6(1-\lambda)E}{5(11+10\lambda)}, \tag{6.2}$$

$$d_{-3,2} = +\frac{(1-\lambda)(1+G)}{6(3+2\lambda)} + \frac{5(18+\lambda-19\lambda^2)E}{21(3+2\lambda)(16+19\lambda)}, \tag{6.3}$$

$$d_{-5,2} = -\frac{(1-\lambda)E}{15(11+10\lambda)}, \tag{6.4}$$

$$e_{-4,2} = +\frac{(1-\lambda)E}{30(5+2\lambda)}. \tag{6.5}$$

And for the internal flow we have

$$b_{2,2} = +\frac{35\lambda E}{(16+19\lambda)}, \tag{6.6}$$

$$d_{2,2} = +\frac{5(1+G)}{12(3+2\lambda)} - \frac{5(1-\lambda)E}{2(3+2\lambda)(16+19\lambda)}, \tag{6.7}$$

https://doi.org/10.1017/jfm.2022.309 Published online by Cambridge University Press

$$d_{4,2} = -\frac{E}{20(11+10\lambda)}, \tag{6.8}$$

$$e_{1,0} = -\frac{(1-G)}{2}, \tag{6.9}$$

$$e_{3,2} = +\frac{7E}{60(5+2\lambda)}. \tag{6.10}$$

Here, the other coefficients vanish, and the e_{ij} values are equal to the those of the previous procedure.

Following Taylor (1934), we represent the surface of the drop and the surface radial velocity at the $z=0$ ($\theta=\pi/2$, $\eta=0$) plane as

$$R(\phi) = 1 + f(\phi), \tag{6.11}$$

so that

$$v_r = \frac{\mathrm{d}R}{\mathrm{d}t} = \frac{\mathrm{d}f}{\mathrm{d}t} = \frac{\mathrm{d}f}{\mathrm{d}\phi}\frac{\mathrm{d}\phi}{\mathrm{d}t}. \tag{6.12}$$

While, on the other hand,

$$v_\phi = r\sin\theta\frac{\mathrm{d}\phi}{\mathrm{d}t} = \frac{\mathrm{d}\phi}{\mathrm{d}t}, \tag{6.13}$$

where the last equality in (6.13) has been evaluated at the surface of the drop ($r=1$) and at the $z=0$ plane. Combining the last two equation results in

$$f(\phi) = \int \frac{v_r}{v_\phi}\,\mathrm{d}\phi. \tag{6.14}$$

Applying a Taylor series on v_r and v_ϕ at $r=1$ and $\theta=\pi/2$ for λ, around $\lambda=\infty$, suggests the following leading-order velocity components:

$$v_r = \frac{5(1+G)}{4\lambda}\sin(2\phi) + \frac{507E}{380\lambda}\sin(2\phi), \tag{6.15}$$

$$v_\phi = -\frac{(1-G)}{2}. \tag{6.16}$$

Substituting the above velocities into (6.14) and then into (6.11) results in an expression for the surface of the drop at the $z=0$ plane, which at first approximation can be described as

$$R = 1 + \frac{5(1+G)}{4\lambda(1-G)}\cos(2\phi) + \frac{507E}{380\lambda(1-G)}\cos(2\phi). \tag{6.17}$$

With an appropriate Taylor deformation parameter of

$$D = \frac{L-B}{L+B} = \left|\frac{5}{4\lambda}\frac{(1+G)}{(1-G)} + \frac{507}{380\lambda}\frac{E}{(1-G)}\right|. \tag{6.18}$$

For the familiar simple (linear) shear flow ($G=0$, $E=0$) in the x-direction, (6.17) and (6.18) reduce to Taylor's results. Clearly, that the treatment presented here, which we suppose to describe small deformations ($f \ll 1$), must be restricted to $\lambda \gg 1$, $Ca = O(1)$, $G = O(1)$ and $E = O(1)$, is independent of Ca and it is not valid for $G \to 1$. When $\lambda \gg 1$ and $G \to 1$, (6.16), as well as the previous treatment, predict, at a leading order, $v_\phi = 0$,

https://doi.org/10.1017/jfm.2022.309 Published online by Cambridge University Press

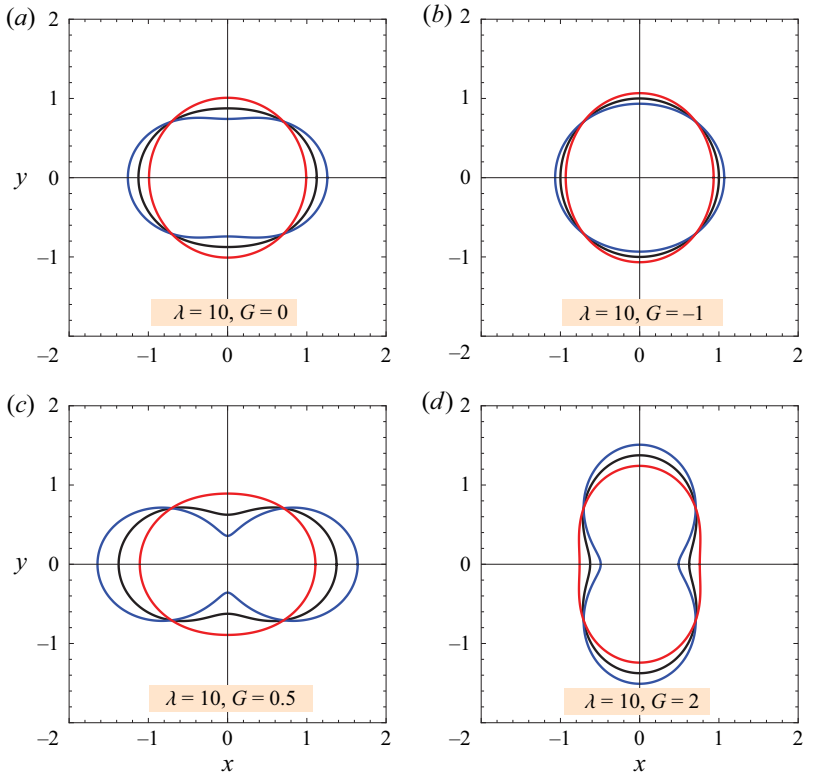


Figure 15. The shape of a very viscous drop with $\lambda = 10$ as a function of G. Black: $E = 0$; blue: $E = 1$; red $E = -1$.

and we may expect the drop to remain at the principal axis of elongation or contraction at $\phi = \pm 45°$.

Figure 15 describes the shape of a viscous drop ($\lambda \gg 1$), at the $z = 0$ plane, for different values of the linear velocity ratio (G), and of the nonlinear intensity of the flow (E). In the first case ($G = 0$), the deformation of the drop appears to increase with E. The largest radius is sometimes aligned with the x axis ($E = 0,\ 1$) and sometimes with the y axis ($E = -1$). The next case ($G = -1$) is interesting. Here, the drop in the linear case ($E = 0$) remains spherical, while the nonlinear cases deform at exactly the same magnitude but at opposite directions. Although difficult to see, for $E = 1$ the largest radius is aligned with the x axis and for $E = -1$ with the y axis. As explained above, under this very viscous drop procedure, the case $G = 1$ is singular, so the last two cases are dedicated to other positive values ($G = 0.5$, $G = 2$). Both cases show a relatively large deformation which increases with E. The difference is in the orientation of the drop. For $G = 0.5$ it is with the x axis, while for $G = 2$ it is with the y axis. Finally, notice that at $\phi = \pm 45°$ and $\pm 135°$, for all cases, the distance of the surface of the drop to the origin is $R = 1$.

7. Conclusions

The fluid mechanics problem of an initially spherical drop subjected to a two-directional nonlinear shear flow, under creeping flow conditions, is theoretical studied. The unperturbed nonlinear shear is a two-dimensional flow, leading to a three-dimensional perturbed motion. Four dimensionless numbers describe this problem: the capillary

https://doi.org/10.1017/jfm.2022.309 Published online by Cambridge University Press

number (Ca), the viscosity ratio (λ), the linear velocity ratio (G) and the nonlinear intensity of the flow (E). By applying Lamb's general solution to the Stokes equations in spherical coordinates, analytical expressions for the external and the internal motion of a spherical drop ($Ca = 0$) have been obtained.

First, we explored the unperturbed motion, that is, the flow in the absence of the drop, given in a dimensionless form by $v_x = y + Ey^3$ and $v_y = Gx + Ex^3$. The velocity components of the two-directional nonlinear shear flow are composed of linear and cubic terms in order to maintain an odd velocity profile around the origin. For a linear shear flow ($E = 0$), if $G = 0$ we have the familiar simple shear flow in the x-direction only with both angular deformation and rotation, if $G = 1$ there is only angular deformation and if $G = -1$ there is rotation only. However, in a nonlinear shear flow ($E \neq 0$), angular deformation and rotation appear simultaneously. The undisturbed nonlinear motion suggests many interesting streamline shapes, as well as up to eight stagnation points, besides the one at the origin, which always is present.

Next, the motion in the presence of a spherical drop ($Ca = 0$) has been examined in detail. For the familiar simple (linear) shear flow ($E = 0$, $G = 0$), we confirmed the detailed work of Bartok & Mason (1958). That is, $\lambda = 0$ is the only case with no closed external streamlines. The internal streamlines suggest: an '8' shape enveloped by an oval shape ($\lambda < 1/2$), an oval shape ($\lambda > 1/2$) and a circular shape ($\lambda \gg 1$). For other combinations of λ, G and E, the internal flow consists of zero, two or four stagnation points (apart from the origin), located at varying distances from the origin, at azimuth angles of $\phi = 0°$, 90°, 180°, 270°, and enclosed by circulations. More stagnation points may appear at the surface of the drop and in the external fluid. When $\lambda = \infty$, the drop becomes a solid sphere and its angular velocity is $\omega = -(1 - G)/2$ independent of E. That is, for $G < 1$ it rotates clockwise, for $G > 1$ it rotates counter-clockwise and for $G = 1$ it does not rotate at all.

In a simple (linear) shear flow ($E = 0$, $G = 0$), the small deformation theory of Taylor, valid for $Ca \ll 1$ and $\lambda = O(1)$, predicts an ellipsoidal drop oriented along the principal axis of elongation at $\phi = 45°$ with the direction of the flow. As Ca increases, the deformation of the drop increases, from spherical to ellipsoidal and finally attains a peanut shape. This peanut shape is also suggested by the $O(Ca^2)$ deformed shape of Barthès-Biesel & Acrivos (1973), and was experimentally observed by Rumscheidt & Mason (1961*b*) and Torza *et al.* (1972) at $\lambda \sim 1$, but may not be physically realized in other cases. In other linear or nonlinear cases, the same behaviour was observed, except for the fact that the drop is sometimes aligned at $\phi = 45°$ and sometimes at $\phi = -45°$, that is, with the principal directions of elongation. When the drop shifts from one orientation to another, it passes via the spherical shape where no deformation is taking place, even at $Ca \neq 0$. The magnitude of the deformation is represented in terms of Taylor's deformation parameter, suggesting that the deformation of the drop is primarily affected by Ca, G and E, while λ variations are of secondary importance.

Taylor observed that small drop deformations are also possible at $Ca = O(1)$ as long as the drop is highly viscous ($\lambda \gg 1$). For the familiar simple (linear) shear flow ($G = 0$, $E = 0$), Taylor's modified his theory to determine that the orientation of the drop is at $\phi = 0°$, that is with the direction of the flow, and its shape is independent of Ca. Accordingly, we followed his solution procedure, and found that, for all linear or nonlinear cases ($G \neq 1$), the orientation of the drop is sometimes at $\phi = 0°$ and sometimes at 90°, independent of Ca.

Finally, we recommend extending this report in two directions. First, an analytical study can be tried, to obtain the $O(Ca^2)$ deformed shape. This will allow us to investigate moderate drop deformations and to have a better description of the drop orientation.

https://doi.org/10.1017/jfm.2022.309 Published online by Cambridge University Press

Second, a numerical investigation using, for example, the boundary integral method, can be performed to provide stronger evidence for our analytical predictions.

The behaviour of emulsions in mixing devices has been extensively modelled in the literature by the deformation and breakup of a single drop in a linear flow, such as axisymmetric extensional flow, hyperbolic flow or simple shear flow. However, mixing devices do not necessarily produce linear flows but rather much more complicated flows in which the velocity vector contains nonlinear terms. Accordingly, the report presented here aimed to explore the influence of a nonlinear shear motion on the behaviour of a single drop embedded in such a flow. Hopefully, the conclusions of this report can improve our understanding of emulsion processing in rotating mixing equipment, where nonlinear flows are expected to be present. The solution method closely followed the classical papers of G.I. Taylor (1932, 1934), which after almost a century, still remain relevant.

Acknowledgements. This research was supported by Shenkar – College of Engineering and Design.

Declaration of interests. The author reports no conflict of interests.

Author ORCIDs.
Moshe Favelukis https://orcid.org/0000-0003-0714-451X.

References

Acrivos, A. 1983 The breakup of small drops and bubbles in shear flows. 4th international conference on physicochemical hydrodynamics. *Ann. N.Y. Acad. Sci.* **404**, 1–11.

Acrivos, A. 1990 Deformation and burst of single drops in shear flows. *AIP Conf.* **197**, 3–6.

Antanovskii, L.K. 1996 Formation of a pointed drop in Taylor's four-roller mill. *J. Fluid Mech.* **327**, 325–341.

Barthès-Biesel, D. & Acrivos, A. 1973 Deformation and burst of a liquid droplet freely suspended in a linear shear field. *J. Fluid Mech.* **61**, 1–21.

Bartok, W. & Mason, S.G. 1958 Particle motion in sheared suspensions. VII. Internal circulation in fluid droplets (theoretical). *J. Colloid Sci.* **13**, 293–307.

Bartok, W. & Mason, S.G. 1959 Particle motion in sheared suspensions. VIII. Singlets and doublets of fluid spheres. *J. Colloid Sci.* **14**, 13–26.

Bentley, B.J. & Leal, L.G. 1986 An experimental investigation of drop deformation and breakup in steady, two-dimensional linear flows. *J. Fluid Mech.* **167**, 241–283.

Briscoe, B.J., Lawrence, C.J. & Mietus, W.G.P. 1999 A review of immiscible fluid mixing. *Adv. Colloid Interface Sci.* **81**, 1–17.

Chaffey, C.E. & Brenner, H. 1967 A second-order theory for shear deformation of drops. *J. Colloid Interface Sci.* **24**, 258–269.

Chaffey, C.E., Brenner, H. & Mason, S.G. 1965*a* Particle motion in sheared suspensions. XVII: deformation and migration of liquid drops. *Rheol. Acta* **4**, 56–63.

Chaffey, C.E., Brenner, H. & Mason, S.G. 1965*b* Particle motion in sheared suspensions. XVIII: wall migration (theoretical). *Rheol. Acta* **4**, 64–72.

Chaffey, C.E., Brenner, H. & Mason, S.G. 1967 Particle motion in sheared suspensions. XVIII: wall migration (theoretical). *Rheol. Acta* **6**, 100.

Chan, P.C.-H. & Leal, L.G. 1979 The motion of a deformable drop in a second-order fluid. *J. Fluid Mech.* **92**, 131–170.

Clift, R., Grace, J.R. & Weber, M.E. 1978 *Bubbles, Drops and Particles*. Academic Press.

Cox, R.G. 1969 The deformation of a drop in a general time-dependent fluid flow. *J. Fluid Mech.* **37**, 601–623.

De Bruijn, R.A. 1993 Tipstreaming of drops in simple shear flows. *Chem. Engng Sci.* **48**, 277–284.

Dimitrakopoulos, P. 2017 Dumbbell formation for elastic capsules in nonlinear extensional Stokes flows. *Phys. Rev. Fluids* **2**, 063101.

Einstein, A. 1906 Eine neue Bestimmung der Moleküldimensionen. *Ann. Phys.* **19**, 289–306.

Einstein, A. 1911 Berichtigung zu meiner Arbeit: Eine neue Bestimmung der Moleküldimensionen. *Ann. Phys.* **34**, 591–592.

Favelukis, M. 2016 A slender drop in a nonlinear extensional flow. *J. Fluid Mech.* **808**, 337–361.

Favelukis, M. 2017 A drop in uniaxial and biaxial nonlinear extensional flows. *Phys. Fluids* **29**, 087102.

https://doi.org/10.1017/jfm.2022.309 Published online by Cambridge University Press

FAVELUKIS, M. 2019*a* Non-Newtonian slender drops in a nonlinear extensional flow. *J. Fluid Mech.* **877**, 561–581.

FAVELUKIS, M. 2019*b* Mass transfer around a slender drop in a nonlinear extensional flow. *Nonlinear Engng* **8**, 117–126.

FAVELUKIS, M. 2019*c* Mass transfer around bubbles, drops, and particles in uniaxial and biaxial nonlinear extensional flows. *AIChE J.* **65**, 398–408.

FAVELUKIS, M. 2020 A compound drop in a nonlinear extensional flow. *Eur. J. Mech.* (B / *Fluids*) **83**, 114–129.

FRANKEL, N.A. & ACRIVOS, A. 1970 The constitutive equation for a dilute emulsion. *J. Fluid Mech.* **44**, 65–78.

GRACE, H.P. 1982 Dispersion phenomena in high viscosity immiscible fluid systems and applications of static mixers as dispersion devices in such systems. *Chem. Engng Commun.* **14**, 225–277.

GUIDO, S. & GRECO, F. 2001 Drop shape under slow steady shear flow and during relaxation. Experimental results and comparison with theory. *Rheol. Acta* **40**, 176–184.

GUIDO, S., GRECO, F. & VILLONE, M. 1999 Experimental determination of drop shape in slow steady shear flow. *J. Colloid Interface Sci.* **219**, 298–309.

GUIDO, S., SIMEONE, M. & ALFANI, A. 2002 Interfacial tension of aqueous mixtures of Na-caseinate and Na-alginate by drop deformation in shear flow. *Carbohyd. Polym.* **48**, 143–152.

HAKIMI, F.S. & SCHOWALTER, W.R. 1980 The effects of shear and vorticity on deformation of a drop. *J. Fluid Mech.* **98**, 635–645.

HAPPEL, J. & BRENNER, H. 1983 *Low Reynolds Number Hydrodynamics*. Kluwer.

HETSRONI, G. & HABER, S. 1970 The flow in and around a droplet or bubble submerged in an unbound arbitrary velocity field. *Rheol. Acta* **9**, 488–496.

KARAM, H.J. & BELLINGER, J.C. 1968 Deformation and breakup of liquid droplets in a simple shear field. *Ind. Engng Chem. Fundam.* **7**, 576–581.

LAMB, H. 1945 *Hydrodynamics*, 6th edn. Dover publications.

LANDAU, L.D. & LIFSHITZ, E.M. 1987 *Fluid Mechanics*, 2nd edn. Pergamon.

LEAL, L.G. 2007 *Advanced Transport Phenomena*. Cambridge University Press.

MEGÍAS-ALGUACIL, D., FEIGL, K., DRESSLER, M., FISCHER, P. & WINDHAB, E.J. 2005 Droplet deformation under simple shear investigated by experiment, numerical simulations and modelling. *J. Non-Newtonian Fluid Mech.* **126**, 153–161.

MEGÍAS-ALGUACIL, D., FISCHER, P. & WINDHAB, E.J. 2004 Experimental determination of interfacial tension by different dynamical methods under simple shear flow conditions with a novel computer-controlled parallel band apparatus. *J. Colloid Interface Sci.* **274**, 631–636.

MEGÍAS-ALGUACIL, D., FISCHER, P. & WINDHAB, E.J. 2006 Determination of the interfacial tension of low density difference liquid-liquid systems containing surfactants by droplet deformation methods. *Chem. Engng Sci.* **61**, 1386–1394.

POLYANIN, A.D., KUTEPOV, A.M., VYAZMIN, A.V. & KAZENIN, D.A. 2002 *Hydrodynamics, Mass and Heat Transfer in Chemical Engineering*. CRC.

POZRIKIDIS, C. 1998 Numerical studies of cusp formation at fluid interfaces in Stokes flow. *J. Fluid Mech.* **357**, 29–57.

RALLISON, J.M. 1980 Note on time-dependent deformation of a viscous drop which is almost spherical. *J. Fluid Mech.* **98**, 625–633.

RALLISON, J.M. 1981 A numerical study of the deformation and burst of a viscous drop in general shear flows. *J. Fluid Mech.* **109**, 465–482.

RALLISON, J.M. 1984 The deformation of small viscous drops and bubbles in shear flows. *Annu. Rev. Fluid Mech.* **16**, 45–66.

RUMSCHEIDT, F.D. & MASON, S.G. 1961*a* Particle motion in sheared suspensions. XI. Internal circulation in fluid droplets (experimental). *J. Colloid Sci.* **16**, 210–237.

RUMSCHEIDT, F.D. & MASON, S.G. 1961*b* Particle motion in sheared suspensions. XII. Deformation and burst of fluid drops in shear and hyperbolic flow. *J. Colloid Sci.* **16**, 238–261.

RUST, A.C. & MANGA, M. 2002 Bubble shapes and orientations in low Re simple shear flow. *J. Colloid Interface Sci.* **249**, 476–480.

SADHAL, S.S., AYYASWAMY, P.S. & CHUNG, J.N. 1997 *Transport Phenomena with Drops and Bubbles.* Springer-Verlag.

SHERWOOD, J.D. 1984 Tip streaming from slender drops in a nonlinear extensional flow. *J. Fluid Mech.* **144**, 281–295.

STONE, H.A. 1994 Dynamics of drop deformation and breakup in viscous fluids. *Annu. Rev. Fluid Mech.* **26**, 65–102.

TAYLOR, G.I. 1932 The viscosity of a fluid containing small drops of another fluid. *Proc. R. Soc.* A **138**, 41–48.

https://doi.org/10.1017/jfm.2022.309 Published online by Cambridge University Press

TAYLOR, G.I. 1934 The formation of emulsions in definable fields of flow. *Proc. R. Soc.* A **146**, 501–523.
TORZA, S., COX, R.G. & MASON, S.G. 1972 Particle motion in sheared suspensions. XXVII: transient and steady deformation and burst of liquid drops. *J. Colloid Interface Sci.* **38**, 395–411.
VANANROYE, A., VAN PUYVELDE, P. & MOLDENAERS, P. 2011 Deformation and orientation of single droplets during shear flow: combined effects of confinement and compatibilization. *Rheol. Acta* **50**, 231–242.
VLAHOVSKA, P.M., BLAWZDZIEWICZ, J. & LOEWENBERG, M. 2009 Small-deformation theory for a surfactant-covered drop in linear flows. *J. Fluid Mech.* **624**, 293–337.
YANG, S.-M. & LEE, T.-Y. 1989 Motions of a fluid drop in linear and quadratic flows. *Korean J. Chem. Engng* **6**, 321–329.
ZAPRYANOV, Z. & TABAKOVA, S. 1999 *Dynamics of Bubbles, Drops and Rigid Particles*. Kluwer Academic Publishers.

https://doi.org/10.1017/jfm.2022.309 Published online by Cambridge University Press